**THE EUROPEAN
PHYSICAL JOURNAL C**

CrossMark

Regular Article - Theoretical Physics

Mueller–Navelet jets at 13 TeV LHC: dependence on dynamic constraints in the central rapidity region

F. G. Celiberto[1,2,a] , **D. Yu. Ivanov**[3,4,b] , **B. Murdaca**[2,c] , **A. Papa**[1,2,d]

[1] Dipartimento di Fisica, Università della Calabria, Arcavacata di Rende, 87036 Cosenza, Italy
[2] Istituto Nazionale di Fisica Nucleare, Gruppo collegato di Cosenza, Arcavacata di Rende, 87036 Cosenza, Italy
[3] Sobolev Institute of Mathematics, 630090 Novosibirsk, Russia
[4] Novosibirsk State University, 630090 Novosibirsk, Russia

Abstract We study the production of Mueller–Navelet jets at 13 TeV LHC, within collinear factorization and including the BFKL resummation of energy logarithms in the next-to-leading approximation. We calculate several azimuthal correlations for different values of the rapidity separation Y between the two jets and evaluate the effect of excluding those events where, for a given Y, one of the two jets is produced in the central region.

1 Introduction

The production at the LHC of Mueller–Navelet jets [1] represents a fundamental test of QCD at high energies. It is an inclusive process where two jets, characterized by large transverse momenta that are of the same order and much larger than Λ_{QCD}, are produced in proton–proton collisions, separated by a large rapidity gap Y and in association with an undetected hadronic system X.

At the LHC energies the rapidity gap between the two jets can be large enough, so that the emission of several undetected hard partons, having large transverse momenta, with rapidities intermediate to those of the two detected jets, becomes possible. The probability of this emission is suppressed in perturbation theory by one power of α_s per produced parton, but when final-state partons are strongly ordered in rapidity, it is also enhanced by large logarithms of the energy which can compensate the smallness of the QCD coupling.

The BFKL approach [2–5] provides with a systematic framework for the resummation of these energy logarithms, both in the leading logarithmic approximation (LLA), which means all terms $(\alpha_s \ln(s))^n$, and in the next-to-leading logarithmic approximation (NLA), which means resummation of all terms $\alpha_s(\alpha_s \ln(s))^n$. In this approach, the cross section for Mueller–Navelet jet production takes the form of a convolution between two impact factors for the transition from each colliding proton to the forward jet (the so-called "jet vertices") and a process-independent Green's function.

The BFKL Green's function obeys an iterative integral equation, whose kernel is known at the next-to-leading order (NLO) both for forward scattering (i.e. for $t = 0$ and color singlet in the t-channel) [6,7] and for any fixed (not growing with energy) momentum transfer t and any possible two-gluon color state in the t-channel [8–12].

The jet vertex can be expressed, within collinear factorization at the leading twist, as the convolution of parton distribution functions (PDFs) of the colliding proton, obeying the standard DGLAP evolution [13–15], with the hard process describing the transition from the parton emitted by the proton to the forward jet in the final state. The Mueller–Navelet jet production process is, therefore, a unique venue, where the two main resummation mechanisms of perturbative QCD play their role at the same time (see Fig. 1 for a schematic view).

The expression for the "jet vertices" was first obtained with NLO accuracy in [16,17], a result later confirmed in [18]. A simpler expression, more practical for numerical purposes, was obtained in [19] within the so-called "small-cone" approximation (SCA) [20–22], i.e. for small jet cone aperture in the rapidity–azimuthal angle plane. The implementation of several jet reconstruction algorithms, both in the exact jet vertex and in its "small-cone" version, has been carried out in [23].

[a] e-mail: francescogiovanni.celiberto@fis.unical.it
[b] e-mail: d-ivanov@math.nsc.ru
[c] e-mail: beatrice.murdaca@cs.infn.it
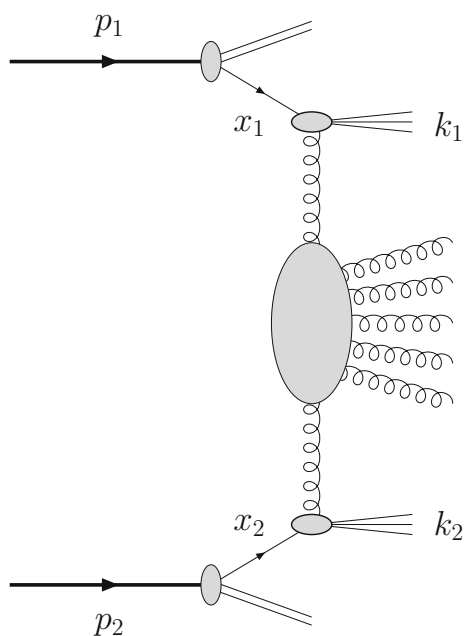[d] e-mails: papa@cs.infn.it; alessandro.papa@fis.unical.it

Fig. 1 Mueller–Navelet jet production process

A lot of papers have appeared, so far, about the Mueller–Navelet jet production process at LHC, both at a center-of-mass energy of 14 TeV [24–26] and 7 TeV [27–31]. Their main aim was the study of the Y-dependence of azimuthal angle correlations between the two measured jets, i.e. average values of $\cos(n\phi)$, where n is an integer and ϕ is the angle in the azimuthal plane between the direction of one jet and the opposite direction of the other jet, and also of ratios of two such cosines [32,33]. These studies share the approach and the factorized form of the basic amplitude, but they differ in the setup of the jet vertex (exact or small-cone approximated) and/or in the procedure to optimize the highly unstable BFKL series.[1] Several possibilities were considered: (i) the inclusion of pieces of the (unknown) next-to-NLO corrections, as dictated by *collinear improvement* [36–46] or by energy-momentum conservation [47], (ii) a suitable choice, within the NLA accuracy, of the renormalization and factorization scales, μ_R and μ_F, and of the BFKL energy scale, s_0, some common options being those inspired by the *principle of minimum sensitivity* (PMS) [48,49], the *fast apparent convergence* (FAC) [50–52] and the *Brodsky–LePage–Mackenzie method* (BLM) [53] (see also Ref. [54]). There is clear evidence that theoretical results can nicely reproduce the CMS data [58] at 7 TeV in the range $5 \lesssim Y \lesssim 9.4$ when the BLM optimization method is adopted, both in the implementation of the amplitude with the exact jet vertex and collinearly

improved BFKL Green's function (see, e.g., Ref. [28]) and with the small-cone jet vertex and no collinear improvement (see Refs. [30,54]), though the experimental uncertainties on the azimuthal correlations and on the PDFs do not allow one to rule out the other optimization procedures. An important clarification could come from the CMS analyses at 13 and 14 TeV, since the larger available energy in the center of mass implies the possibility of a larger average number of parton emission between the jets and, hence, better conditions for the manifestation of the BFKL dynamics. Moreover, some added information could come (i) from the measurement, in addition to azimuthal correlations, of the total cross section for Mueller–Navelet jets and (ii) from the consideration of asymmetric cuts in the transverse momenta of the two detected jets. It was indeed shown in Ref. [30] that the total cross section is much more sensitive to the optimization procedure than azimuthal correlations and is, therefore, a better discriminator of the various options. It was also discussed that the use of asymmetric cuts in jet transverse momenta allows for a better separation between BFKL-resummed and fixed-order predictions in azimuthal correlations and their ratios, as was indeed shown in Ref. [31].

There is another issue which deserves some care and has not been taken into consideration both in theoretical and experimental analyses so far. As discussed in the last Section of Ref. [30], in defining the Y value for a given final state with two jets, the rapidity of one of the two jets could be so small, say $|y_i| \lesssim 2$, that this jet is actually produced in the central region, rather than in one of the two forward regions. Since the longitudinal momentum fractions of the parent partons x that generate such a central jet are very small, one can naturally expect sizable corrections to the vertex of this jet, due to the fact that the collinear factorization approach used in the derivation of the result for jet vertex could not be accurate enough in our kinematic region, where the x values can be as small as $x \sim 10^{-3}$.

The use of collinear factorization methods in the case of central jet production in our kinematic range deserves some discussion. On one hand, at $x \sim 10^{-3}$ and at scales of the order of the jet transverse momenta which we consider here, $\sim 20 \div 40$ GeV, PDFs are well constrained, mainly from DIS HERA data. On the other hand, in this kinematic region PDF parametrizations extracted in NNLO and in NLO approximations start to differ one from the other, which indicates that NNLO effects become essential in the DIS cross sections. The situation with central jet production in proton–proton collisions may be different. Recently in [55] results for NNLO corrections to the dijet production originating from the gluonic subprocesses were presented. In the region $|y_{1,2}| < 0.3$ and for jet transverse momenta ~ 100 GeV, the account of NNLO effects leads to an increase of the cross section by $\sim 25\%$. For our kinematics, featuring smaller jet transverse momenta and "less inclusive" cover-

---

[1] It is worth mentioning two recent studies, Refs. [34,35], which considered, respectively, the contribution to Mueller–Navelet jet production from the double-parton exchange mechanism and from Sudakov resummations.

age of jet rapidities, one could expect even larger NNLO corrections.

Conceptually, instead of the collinear approach, for jets produced in the central rapidity region (at very small x) a promising approach would be to use a high-energy factorization scheme (often also referred as k_T-factorization) together with the NLO central jet vertex calculated in [56].[2]

Returning back to our case of Mueller–Navelet jets, we see here as an important task to reveal dynamic mechanisms for the partonic interaction in the semihard region, $s \gg |t|$, comparing theory predictions with data. From the theory side we have now the BFKL approach, where one can resum in a model-independent way only the leading and first subleading logarithms of the energy. Several approaches to handle big effects beyond the NLA BFKL were suggested, such as the above-discussed collinear improvement, BLM, and so on. The comparison of theory predictions with experiment should clarify what is the better approach. For this reason we suggest to compare BFKL theory predictions with data in a region where theoretical uncertainties related with other kind of physics are most possibly reduced. Therefore we propose to return to the original Mueller–Navelet idea, to study the inclusive production of two forward jets separated by a large rapidity gap, and to remove from the analysis those regions where jets are produced at central rapidities.

As a contribution to the assessment of this effect, in this paper we will study the Y-dependence of several azimuthal correlations and ratios among them, imposing the additional constraint that the rapidity of a Mueller–Navelet jet cannot be smaller than a given value. Then we will compare this option with the case when the constraint is absent.

Since here we want to focus just on the possible impact of jets produced in the central region, we will stick to a definite optimization setup, namely the BLM one, which performed quite successfully in the comparison with CMS data at 7 TeV. We will implement its "exact" version, according to the nomenclature introduced in Ref. [54] and fix the center-of-mass energy at 13 TeV, so that our results can be directly compared with the forthcoming CMS analyses.

The paper is organized as follows: in the next section we recall the kinematics and the basic formulas for the Mueller–Navelet jet process cross section; in Sect. 3 we present our results; finally, in Sect. 4 we draw our conclusions.

2 Theoretical setup

In this section we briefly recall the kinematics of the process and the main formulas, referring the reader to Refs. [25,30] for the omitted details.

---

[2] For the discussion of different approaches to factorization for dijet production see, e.g., the recent review paper [57].

The process under exam is the production of Mueller–Navelet jets [1] in proton–proton collisions

$$p(p_1) + p(p_2) \to \mathrm{jet}(k_{J_1}) + \mathrm{jet}(k_{J_2}) + X, \tag{1}$$

where the two jets are characterized by high transverse momenta, $\vec{k}_{J_1}^2 \sim \vec{k}_{J_2}^2 \gg \Lambda_{\mathrm{QCD}}^2$ and large separation in rapidity; p_1 and p_2 are taken as Sudakov vectors satisfying $p_1^2 = p_2^2 = 0$ and $2(p_1 p_2) = s$, working at leading twist and neglecting the proton mass and other power suppressed corrections.

In QCD collinear factorization the cross section of the process (1) reads

$$\frac{\mathrm{d}\sigma}{\mathrm{d}x_{J_1}\mathrm{d}x_{J_2}\mathrm{d}^2 k_{J_1}\mathrm{d}^2 k_{J_2}} = \sum_{i,j=q,\bar{q},g} \int_0^1 \mathrm{d}x_1 \int_0^1 \mathrm{d}x_2$$

$$\times f_i(x_1,\mu_F) f_j(x_2,\mu_F) \frac{\mathrm{d}\hat{\sigma}_{i,j}(x_1 x_2 s,\mu_F)}{\mathrm{d}x_{J_1}\mathrm{d}x_{J_2}\mathrm{d}^2 k_{J_1}\mathrm{d}^2 k_{J_2}}, \tag{2}$$

where the i, j indices specify the parton types (quarks $q = u, d, s, c, b$; antiquarks $\bar{q} = \bar{u}, \bar{d}, \bar{s}, \bar{c}, \bar{b}$; or gluon g), $f_i(x, \mu_F)$ denotes the initial proton PDFs; $x_{1,2}$ are the longitudinal fractions of the partons involved in the hard subprocess, while $x_{J_{1,2}}$ are the jet longitudinal fractions; μ_F is the factorization scale; $\mathrm{d}\hat{\sigma}_{i,j}(x_1 x_2 s, \mu_F)$ is the partonic cross section for the production of jets and $x_1 x_2 s \equiv \hat{s}$ is the squared center-of-mass energy of the parton–parton collision subprocess (see Fig. 1).

The cross section of the process can be represented as

$$\frac{\mathrm{d}\sigma}{\mathrm{d}y_{J_1}\mathrm{d}y_{J_2}\,\mathrm{d}|\vec{k}_{J_1}|\,\mathrm{d}|\vec{k}_{J_2}|\mathrm{d}\phi_{J_1}\mathrm{d}\phi_{J_2}}$$

$$= \frac{1}{(2\pi)^2}\left[\mathcal{C}_0 + \sum_{n=1}^{\infty} 2\cos(n\phi)\,\mathcal{C}_n\right], \tag{3}$$

where $\phi = \phi_{J_1} - \phi_{J_2} - \pi$, while $\mathcal{C}_0$ gives the total cross section and the other coefficients $\mathcal{C}_n$ determine the distribution of the azimuthal angle of the two jets.

Since the main object of the present analysis is the impact of jet produced in the central region on azimuthal coefficients, we will adopt just one representation for $\mathcal{C}_n$, out of the many possible NLA-equivalent options (see Ref. [30] for a discussion). In particular, we will use the so-called *exponentiated* representation together with the BLM optimization method to fix the common value for the renormalization scale μ_R and the factorization scale μ_F. In [30] it was shown that this setup allows a nice agreement with CMS data for several azimuthal correlations and their ratios in the large Y regime. In our calculation we will use "exact" and in some cases also approximate, semianalytic implementations of BLM method, which are called below (a), (b) cases, in order to keep contact with previous applications of the BLM method where approximate approaches were used; for the details see Ref. [54].

Introducing, for the sake of brevity, the definitions

$$Y = y_1 - y_2 = \ln \frac{x_{J_1} x_{J_2} s}{|\vec{k}_{J_1}||\vec{k}_{J_2}|}, \qquad Y_0 = \ln \frac{s_0}{|\vec{k}_{J_1}||\vec{k}_{J_2}|},$$

we will present in the following the three different expressions for the coefficients $\mathcal{C}_n$.

- case "exact"

  The BLM optimal scale μ_R^{BLM} is defined as the value of μ_R that makes all contributions to the considered observables which are proportional to the QCD β-function, β_0, vanish. In our case we have

$$
\begin{aligned}
\mathcal{C}_n^\beta \equiv{} & \frac{x_{J_1} x_{J_2}}{|\vec{k}_{J_1}||\vec{k}_{J_2}|} \int_{-\infty}^{\infty} d\nu \left(\frac{s}{s_0}\right)^{\bar{\alpha}_s^{\text{MOM}}(\mu_R^{\text{BLM}})\chi(n,\nu)} \left(\alpha_s^{\text{MOM}}(\mu_R^{\text{BLM}})\right)^3 \\
& \times c_1(n,\nu) c_2(n,\nu) \frac{\beta_0}{2N_c} \left[\frac{5}{3} + \ln \frac{(\mu_R^{\text{BLM}})^2}{|\mathbf{k}_{J_1}||\mathbf{k}_{J_2}|} - 2\left(1 + \frac{2}{3}I\right)\right] \\
& + \bar{\alpha}_s^{\text{MOM}}(\mu_R^{\text{BLM}}) \ln \frac{s}{s_0} \frac{\chi(n,\nu)}{2} \\
& \times \left(-\frac{\chi(n,\nu)}{2} + \frac{5}{3} + \ln \frac{(\mu_R^{\text{BLM}})^2}{Q_1 Q_2} - 2\left(1 + \frac{2}{3}I\right)\right)\right] = 0.
\end{aligned}
$$
(4)

The first term in the r.h.s. of Eq. (4) originates from the NLO correction to the jet vertices, whereas the second, $\sim\alpha^{\text{MOM}}$, contribution is due to the $\sim\beta_0$ part of NLO correction to the kernel of the BFKL equation.

In [54] we considered the implementation of the BLM method for general semihard process. We found that the above-mentioned $\sim\beta_0$-contributions to the NLO impact factors are universally expressed in terms of the LO impact factors of the considered process (the LO jet vertices for the Mueller–Navelet process considered here). Such contributions must be taken into account in the implementation of BLM method, because *all* contributions to the cross section that are $\sim\beta_0$ must vanish at the BLM scale.

After that we have the following expression for our observables:

$$
\begin{aligned}
\mathcal{C}_n^{\text{BLM}} ={} & \frac{x_{J_1} x_{J_2}}{|\vec{k}_{J_1}||\vec{k}_{J_2}|} \int_{-\infty}^{+\infty} d\nu \, e^{(Y-Y_0)\bar{\alpha}_s^{\text{MOM}}(\mu_R^{\text{BLM}})\left[\chi(n,\nu) + \bar{\alpha}_s^{\text{MOM}}(\mu_R^{\text{BLM}})\left(\bar{\chi}(n,\nu) + \frac{T^{\text{conf}}}{N_c}\chi(n,\nu)\right)\right]} \\
& \times (\alpha_s^{\text{MOM}}(\mu_R^{\text{BLM}}))^2 c_1(n,\nu,|\vec{k}_{J_1}|,x_{J_1}) c_2(n,\nu,|\vec{k}_{J_2}|,x_{J_2}) \\
& \times \left[1 + \alpha_s^{\text{MOM}}(\mu_R^{\text{BLM}})\left\{\frac{\bar{c}_1^{(1)}(n,\nu,|\vec{k}_{J_1}|,x_{J_1})}{c_1(n,\nu,|\vec{k}_{J_1}|,x_{J_1})} + \frac{\bar{c}_2^{(1)}(n,\nu,|\vec{k}_{J_2}|,x_{J_2})}{c_2(n,\nu,|\vec{k}_{J_2}|,x_{J_2})} + \frac{2T^{\text{conf}}}{N_c}\right\}\right].
\end{aligned}
$$
(5)

In the above equations, $\bar{\alpha}_s^{\text{MOM}} \equiv \alpha_s^{\text{MOM}} N_c/\pi$, with N_c the number of colors and α_s^{MOM} is the QCD coupling in the physical momentum subtraction (MOM) scheme, related to $\alpha_s^{\overline{\text{MS}}}$ by a finite renormalization,

$$\alpha_s^{\overline{\text{MS}}} = \alpha_s^{\text{MOM}} \left(1 + \frac{\alpha_s^{\text{MOM}}}{\pi} T\right),$$
(6)

with $T = T^\beta + T^{\text{conf}}$,

$$T^\beta = -\frac{\beta_0}{2}\left(1 + \frac{2}{3}I\right),$$
(7)

$$T^{\text{conf}} = \frac{N_c}{8}\left[\frac{17}{2}I + \frac{3}{2}(I-1)\xi + \left(1 - \frac{1}{3}I\right)\xi^2 - \frac{1}{6}\xi^3\right],$$

where $I = -2\int_0^1 dx \frac{\ln(x)}{x^2-x+1} \simeq 2.3439$ and ξ is a gauge parameter, fixed at zero in the following. Then

$$\beta_0 = \frac{11}{3}N_c - \frac{2}{3}n_f$$
(8)

is the first coefficient of the QCD β-function,

$$\chi(n,\nu) = 2\psi(1) - \psi\left(\frac{n}{2} + \frac{1}{2} + i\nu\right) - \psi\left(\frac{n}{2} + \frac{1}{2} - i\nu\right)$$
(9)

is the LO BFKL characteristic function,

$$
\begin{aligned}
c_1(n,\nu,|\vec{k}|,x) ={} & 2\sqrt{\frac{C_F}{C_A}}(\vec{k}^2)^{i\nu-1/2} \\
& \times \left(\frac{C_A}{C_F} f_g(x,\mu_F) + \sum_{a=q,\bar{q}} f_a(x,\mu_F)\right)
\end{aligned}
$$
(10)

and

$$c_2(n,\nu,|\vec{k}|,x) = \left[c_1(n,\nu,|\vec{k}|,x)\right]^*,$$
(11)

are the LO jet vertices in the ν-representation. The remaining objects are related with the NLO corrections of the BFKL kernel ($\bar{\chi}(n,\nu)$, given in Eqs. (23) of Ref. [25]) and of the jet vertices in the small-cone approximation ($c_{1,2}^{(1)}(n,\nu,|\vec{k}_{J_{1,2}}|,x_{J_{1,2}})$, given in Eqs. (36) and (37) of Ref. [25]). The functions $\bar{c}_{1,2}^{(1)}(n,\nu,|\vec{k}_{J_2}|,x_{J_2})$ are the same as $c_{1,2}^{(1)}(n,\nu,|\vec{k}_{J_{1,2}}|,x_{J_{1,2}})$ with all terms proportional to β_0 removed.

Note that the "exact" implementation of the BLM method requires numerical solution of an integral equation, Eq. (4)

for each value of s and the values of μ_R^{BLM} obtained in this way depend on the energy of the process.

Below we will perform also calculations with two approximated approaches to the BLM scale setting. We will consider the options where μ_R is chosen such that in the r.h.s. of Eq. (4) either the term coming from the NLO correction to the jet vertices vanishes [case (a)], or the contribution due to the $\sim \beta_0$ part of NLO BFKL kernel does [case (b)]. In these two cases one gets simpler analytical expressions for the BLM scales which do not depend on the energy. Such approximate approaches were used earlier in the literature of the BLM method for different semihard processes (see a more detailed discussion in [54]). Here we will perform also some calculations with these approximate schemes (a) and (b), in order to get an idea about the inaccuracy of the predictions for Mueller–Navelet jets observables related with such approximate implementations of the BLM scale setting.

So, we have:

• case (a)

$$(\mu_{R,a}^{\mathrm{BLM}})^2 = k_{J_1} k_{J_2} \exp\left[2\left(1 + \frac{2}{3}I\right) - \frac{5}{3}\right],$$

with

$$
\mathcal{C}_n^{\mathrm{BLM},a} = \frac{x_{J_1} x_{J_2}}{|\vec{k}_{J_1}||\vec{k}_{J_2}|} \int_{-\infty}^{+\infty} d\nu\, e^{(Y-Y_0)\left[\bar{\alpha}_s^{\mathrm{MOM}}(\mu_{R,a}^{\mathrm{BLM}})\chi(n,\nu) + (\bar{\alpha}_s^{\mathrm{MOM}}(\mu_{R,a}^{\mathrm{BLM}}))^2\left(\bar{\chi}(n,\nu) + \frac{T^{\mathrm{conf}}}{N_c}\chi(n,\nu) - \frac{\beta_0}{8N_c}\chi^2(n,\nu)\right)\right]}
$$
$$
\times (\alpha_s^{\mathrm{MOM}}(\mu_{R,a}^{\mathrm{BLM}}))^2 c_1(n,\nu,|\vec{k}_{J_1}|,x_{J_1}) c_2(n,\nu,|\vec{k}_{J_2}|,x_{J_2})
$$
$$
\times \left[1 + \alpha_s^{\mathrm{MOM}}(\mu_{R,a}^{\mathrm{BLM}})\left\{\frac{\bar{c}_1^{(1)}(n,\nu,|\vec{k}_{J_1}|,x_{J_1})}{c_1(n,\nu,|\vec{k}_{J_1}|,x_{J_1})} + \frac{\bar{c}_2^{(1)}(n,\nu,|\vec{k}_{J_2}|,x_{J_2})}{c_2(n,\nu,|\vec{k}_{J_2}|,x_{J_2})} + \frac{2T^{\mathrm{conf}}}{N_c}\right\}\right], \tag{12}
$$

and

• case (b)

$$(\mu_{R,b}^{\mathrm{BLM}})^2 = k_{J_1} k_{J_2} \exp\left[2\left(1 + \frac{2}{3}I\right) - \frac{5}{3} + \frac{1}{2}\chi(n,\nu)\right],$$

with

$$
\mathcal{C}_n^{\mathrm{BLM},b} = \frac{x_{J_1} x_{J_2}}{|\vec{k}_{J_1}||\vec{k}_{J_2}|} \int_{-\infty}^{+\infty} d\nu\, e^{(Y-Y_0)\left[\bar{\alpha}_s^{\mathrm{MOM}}(\mu_{R,b}^{\mathrm{BLM}})\chi(n,\nu) + (\bar{\alpha}_s^{\mathrm{MOM}}(\mu_{R,b}^{\mathrm{BLM}}))^2\left(\bar{\chi}(n,\nu) + \frac{T^{\mathrm{conf}}}{N_c}\chi(n,\nu)\right)\right]}
$$
$$
\times (\alpha_s^{\mathrm{MOM}}(\mu_{R,b}^{\mathrm{BLM}}))^2 c_1(n,\nu,|\vec{k}_{J_1}|,x_{J_1}) c_2(n,\nu,|\vec{k}_{J_2}|,x_{J_2})
$$
$$
\times \left[1 + \alpha_s^{\mathrm{MOM}}(\mu_{R,b}^{\mathrm{BLM}})\left\{\frac{\bar{c}_1^{(1)}(n,\nu,|\vec{k}_{J_1}|,x_{J_1})}{c_1(n,\nu,|\vec{k}_{J_1}|,x_{J_1})} + \frac{\bar{c}_2^{(1)}(n,\nu,|\vec{k}_{J_2}|,x_{J_2})}{c_2(n,\nu,|\vec{k}_{J_2}|,x_{J_2})} + \frac{2T^{\mathrm{conf}}}{N_c} + \frac{\beta_0}{4N_c}\chi(n,\nu)\right\}\right]. \tag{13}
$$

Note that in the above equations the scale s_0 entering Y_0 is the artificial energy scale introduced in the BFKL approach to perform the Mellin transform from the s-space to the complex angular momentum plane and cancels in the full expression, up to terms beyond the NLA. In the following it will always be fixed at the "natural" value $Y_0 = 0$, given by the kinematic of Mueller–Navelet process.

3 Numerical analysis

In this section we present our results for the dependence on the rapidity separation between the detected jets, $Y = y_{J_1} - y_{J_2}$, of ratios $\mathcal{R}_{nm} \equiv C_n/C_m$ between the coefficients C_n. Among them, the ratios of the form R_{n0} have a simple physical interpretation, being the azimuthal correlations $\langle\cos(n\phi)\rangle$.

In order to match the kinematic cuts used by the CMS collaboration, we will consider the *integrated coefficients* given by

$$
C_n = \int_{y_{1,\min}}^{y_{1,\max}} dy_1 \int_{y_{2,\min}}^{y_{2,\max}} dy_2 \int_{k_{J_1,\min}}^{\infty} dk_{J_1} \int_{k_{J_2,\min}}^{\infty} dk_{J_2}
$$
$$
\times \delta(y_1 - y_2 - Y)\,\theta\left(|y_1| - y_{\max}^{\mathrm{C}}\right)\theta\left(|y_2| - y_{\max}^{\mathrm{C}}\right)
$$
$$
\times \mathcal{C}_n\left(y_{J_1}, y_{J_2}, k_{J_1}, k_{J_2}\right) \tag{14}
$$

and their ratios $R_{nm} \equiv C_n/C_m$. In Eq. (14), the two step-functions force the exclusion of jets whose rapidity is smaller than a cutoff value, given by $y_{\max}^{\mathrm{C}}$, which delimits the central rapidity region. We will take jet rapidities in the range delimited by $y_{1,\min} = y_{2,\min} = -4.7$ and $y_{1,\max} = y_{2,\max} = 4.7$, as in the CMS analyses at 7 TeV, and consider $Y = 3.5, 4.5, 5.5, 6.5, 7.5, 8.5, 9.0$.

As for the values of $y_{\max}^{\mathrm{C}}$, we will consider three cases: $y_{\max}^{\mathrm{C}} = 0$, which means no exclusion from jets in the central

Table 1 C_0 [nb] and ratios C_n/C_m for $k_{J_1,\min} = k_{J_2,\min} = 20\,\text{GeV}$ and $y^C_{\max} = 2.5$, for the three variants of the BLM method (see Fig. 2)

	Y	BLM_a	BLM_b	$\text{BLM}_{\text{exact}}$
C_0	5.5	1353.2 (5.6)	1413.2 (3.2)	1318 (16)
	6.5	1778 (23)	1877 (13)	1720 (49)
	7.5	834.6 (2.8)	893.7 (2.0)	803.4 (6.6)
	8.5	140.06 (25)	152.03 (18)	133.91 (78)
	9.0	32.97 (10)	36.16 (12)	31.46 (20)
C_1/C_0	5.5	0.7641 (68)	0.7434 (37)	0.775 (19)
	6.5	0.674 (17)	0.6546 (87)	0.686 (37)
	7.5	0.6005 (44)	0.5775 (22)	0.6104 (99)
	8.5	0.5339 (19)	0.5092 (11)	0.5422 (64)
	9.0	0.5091 (27)	0.4823 (23)	0.5174 (65)
C_2/C_0	5.5	0.4371 (52)	0.4315 (29)	0.450 (18)
	6.5	0.336 (11)	0.3357 (53)	0.3329 (19)
	7.5	0.2638 (27)	0.2625 (13)	0.2611 (35)
	8.5	0.2052 (11)	0.20452 (59)	0.1939 (49)
	9.0	0.1835 (14)	0.1827 (11)	0.1674 (14)
C_3/C_0	5.5	0.2761 (45)	0.2691 (26)	0.3019 (68)
	6.5	0.1934 (74)	0.1907 (37)	0.210 (18)
	7.5	0.1383 (20)	0.13708 (80)	0.144 (29)
	8.5	0.09796 (70)	0.09765 (31)	0.095 (17)
	9.0	0.08378 (90)	0.08361 (63)	0.0775 (13)
C_2/C_1	5.5	0.5721 (71)	0.5804 (42)	0.580 (24)
	6.5	0.499 (15)	0.5128 (76)	0.484 (27)
	7.5	0.4393 (47)	0.4546 (19)	0.4278 (55)
	8.5	0.3844 (21)	0.4017 (11)	0.3576 (91)
	9.0	0.3605 (23)	0.3788 (19)	0.3236 (27)
C_3/C_2	5.5	0.632 (13)	0.6236 (74)	0.671 (26)
	6.5	0.575 (25)	0.568 (12)	0.634 (55)
	7.5	0.5241 (93)	0.5221 (32)	0.5509 (92)
	8.5	0.4773 (41)	0.4775 (18)	0.492 (16)
	9.0	0.4565 (55)	0.4577 (29)	0.4627 (59)

Table 2 Values of C_0 [nb] from the "exact" BLM method, for all choices of the cuts on jet transverse momenta and of the central rapidity region (see Fig. 3)

$k_{J_1,\min}$ (GeV)	$k_{J_2,\min}$ (GeV)	Y	$y^C_{\max} = 0$	$y^C_{\max} = 1.5$	$y^C_{\max} = 2.5$
20	20	3.5	46,100 (950)	5498 (110)	–
		4.5	20,410 (290)	8200 (130)	–
		5.5	8270 (130)	6120 (110)	1318 (16)
		6.5	2902 (31)	2902 (31)	1720 (49)
		7.5	803.4 (6.6)	803.4 (6.6)	803.4 (6.6)
		8.5	133.91 (78)	133.91 (78)	133.91 (78)
		9.0	31.46 (20)	31.46 (20)	31.46 (20)
20	30	3.5	15,000 (270)	1842 (27)	–
		4.5	6734 (73)	2779 (33)	–
		5.5	2701 (51)	2030 (34)	442.3 (3.4)
		6.5	919.8 (9.2)	919.8 (9.2)	555 (13)
		7.5	240.8 (1.6)	240.8 (1.6)	240.8 (1.6)
		8.5	36.44 (13)	36.44 (13)	36.44 (13)
		9.0	7.801 (53)	7.801 (53)	7.801 (53)
20	35	3.5	8090 (160)	1050 (20)	–
		4.5	3793 (54)	1598 (21)	–
		5.5	1534 (26)	1169 (16)	256.0 (2.1)
		6.5	520.6 (6.2)	520.6 (6.2)	318.5 (6.9)
		7.5	134.2 (1.1)	134.2 (1.1)	134.2 (1.1)
		8.5	19.422 (98)	19.422 (98)	19.422 (98)
		9.0	3.9601 (23)	3.9601 (23)	3.9601 (23)
20	40	3.5	4627 (86)	595.3 (7.3)	–
		4.5	2137 (31)	912 (10)	–
		5.5	872 (13)	668 (10)	146.68 (94)
		6.5	295.4 (2.7)	295.4 (2.7)	181.6 (4.1)
		7.5	74.75 (37)	74.75 (37)	74.75 (37)
		8.5	10.362 (30)	10.362 (30)	10.362 (30)
		9.0	1.9980 (45)	1.9980 (45)	1.9980 (45)
35	35	3.5	4286 (36)	544.7 (6.0)	–
		4.5	1618 (13)	690.9 (3.3)	–
		5.5	555.2 (4.1)	429.0 (3.6)	94.48 (13)
		6.5	161.8 (1.2)	161.8 (1.2)	101.5 (1.1)
		7.5	35.70 (16)	35.70 (16)	35.70 (16)
		8.5	4.2843 (98)	4.2843 (98)	4.2843 (98)
		9.0	0.7579 (23)	0.7579 (23)	0.7579 (23)

region, as in all the numerical analyses so far; $y^C_{\max} = 1.5$, corresponding to a central region with size equal to about one third of the maximum possible rapidity span $Y = 9.4$ and $y^C_{\max} = 2.5$, as a control value, to check the stability of our results.

Concerning the jet transverse momenta, differently from most previous analyses, we make the following five choices, which include *asymmetric* cuts: (1) $k_{J_1,\min} = 20\,\text{GeV}$, $k_{J_2,\min} = 20\,\text{GeV}$, (2) $k_{J_1,\min} = 20\,\text{GeV}$, $k_{J_2,\min} = 30\,\text{GeV}$, (3) $k_{J_1,\min} = 20\,\text{GeV}$, $k_{J_2,\min} = 35\,\text{GeV}$, (4) $k_{J_1,\min} = 20\,\text{GeV}$, $k_{J_2,\min} = 40\,\text{GeV}$, and (5) $k_{J_1,\min} = 35\,\text{GeV}$, $k_{J_2,\min} = 35\,\text{GeV}$. The jet cone size R entering the NLO-jet vertices is fixed at the value $R = 0.5$, the center-of-mass energy at $\sqrt{s} = 13\,\text{TeV}$ and, as anticipated, $Y_0 = 0$. We use the PDF set MSTW 2008 NLO [59] and the two-loop running coupling with $\alpha_s(M_Z) = 0.11707$. The MSTW 2008

NLO PDF set was used successfully in various analyses of inclusive jet production at LHC, including our previous studies of Mueller–Navelet jets. Now there exist updated PDF parametrizations, including the MMHT 2014 set [60], which is the successor of the MSTW 2008 analysis. Here we continue to use MSTW 2008 NLO PDFs because in our kinematic range the difference between MSTW 2008 NLO and the updated MMHT 2014 NLO PDFs is very small. Also, we want to keep the opportunity to compare our results at 13 TeV

Table 3 Values of C_1/C_0 from the "exact" BLM method, for all choices of the cuts on jet transverse momenta and of the central rapidity region (see Fig. 4)

$k_{J_1,\min}$ (GeV)	$k_{J_2,\min}$ (GeV)	Y	$y_{\max}^C = 0$	$y_{\max}^C = 1.5$	$y_{\max}^C = 2.5$
20	20	3.5	0.988 (37)	0.975 (35)	–
		4.5	0.885 (25)	0.874 (27)	–
		5.5	0.785 (25)	0.778 (31)	0.775 (19)
		6.5	0.692 (18)	0.692 (18)	0.686 (37)
		7.5	0.6104 (99)	0.6104 (99)	0.6104 (99)
		8.5	0.5423 (64)	0.5423 (64)	0.5423 (64)
		9.0	0.5174 (64)	0.5174 (64)	0.5174 (64)
20	30	3.5	1.004 (31)	0.989 (28)	–
		4.5	0.896 (18)	0.886 (20)	–
		5.5	0.799 (27)	0.792 (27)	0.783 (10)
		6.5	0.710 (13)	0.710 (13)	0.702 (33)
		7.5	0.6321 (83)	0.6321 (83)	0.6321 (83)
		8.5	0.5717 (45)	0.5717 (45)	0.5717 (45)
		9.0	0.5543 (70)	0.5543 (70)	0.5543 (70)
20	35	3.5	1.051 (37)	1.005 (33)	–
		4.5	0.907 (24)	0.892 (24)	–
		5.5	0.803 (28)	0.795 (22)	0.788 (13)
		6.5	0.712 (16)	0.712 (16)	0.704 (31)
		7.5	0.636 (10)	0.636 (10)	0.636 (10)
		8.5	0.5803 (56)	0.5803 (56)	0.5803 (56)
		9.0	0.5679 (74)	0.5679 (74)	0.5679 (74)
20	40	3.5	1.043 (35)	1.021 (22)	–
		4.5	0.916 (25)	0.899 (20)	–
		5.5	0.808 (22)	0.798 (24)	0.791 (10)
		6.5	0.714 (12)	0.714 (12)	0.705 (31)
		7.5	0.6383 (64)	0.6383 (64)	0.6383 (64)
		8.5	0.5875 (35)	0.5875 (35)	0.5875 (35)
		9.0	0.5804 (25)	0.5804 (25)	0.5804 (25)
35	35	3.5	0.963 (16)	0.952 (18)	–
		4.5	0.883 (14)	0.8722 (82)	–
		5.5	0.798 (13)	0.792 (12)	0.7866 (22)
		6.5	0.718 (11)	0.718 (11)	0.709 (16)
		7.5	0.6478 (53)	0.6478 (53)	0.6478 (53)
		8.5	0.5972 (26)	0.5972 (26)	0.5972 (26)
		9.0	0.5886 (33)	0.5886 (33)	0.5886 (33)

Table 4 Values of C_2/C_0 from the "exact" BLM method, for all choices of the cuts on jet transverse momenta and of the central rapidity region (see Fig. 5)

$k_{J_1,\min}$ (GeV)	$k_{J_2,\min}$ (GeV)	Y	$y_{\max}^C = 0$	$y_{\max}^C = 1.5$	$y_{\max}^C = 2.5$
20	20	3.5	0.749 (25)	0.730 (30)	–
		4.5	0.594 (23)	0.581 (24)	–
		5.5	0.458 (13)	0.454 (27)	0.450 (18)
		6.5	0.350 (13)	0.350 (13)	0.332 (19)
		7.5	0.2611 (35)	0.2611 (35)	0.2611 (35)
		8.5	0.1939 (49)	0.1939 (49)	0.1939 (49)
		9.0	0.1674 (14)	0.1674 (14)	0.1674 (14)
20	30	3.5	0.727 (27)	0.719 (26)	–
		4.5	0.575 (15)	0.565 (17)	–
		5.5	0.450 (20)	0.443 (21)	0.4398 (98)
		6.5	0.3483 (94)	0.3483 (94)	0.343 (24)
		7.5	0.2683 (53)	0.2683 (53)	0.2683 (53)
		8.5	0.2083 (30)	0.2083 (30)	0.2083 (30)
		9.0	0.1872 (39)	0.1872 (39)	0.1872 (39)
20	35	3.5	0.750 (22)	0.714 (29)	–
		4.5	0.563 (20)	0.555 (20)	–
		5.5	0.435 (11)	0.430 (17)	0.4268 (40)
		6.5	0.337 (12)	0.337 (12)	0.331 (20)
		7.5	0.2602 (32)	0.2602 (32)	0.2602 (32)
		8.5	0.2059 (37)	0.2059 (37)	0.2059 (37)
		9.0	0.1874 (15)	0.1874 (15)	0.1874 (15)
20	40	3.5	0.727 (21)	0.710 (19)	–
		4.5	0.560 (17)	0.546 (16)	–
		5.5	0.4225 (99)	0.420 (20)	0.4158 (75)
		6.5	0.3276 (91)	0.3276 (91)	0.321 (23)
		7.5	0.2528 (22)	0.2528 (22)	0.2528 (22)
		8.5	0.2021 (26)	0.2021 (26)	0.2021 (26)
		9.0	0.18712 (7)	0.18712 (7)	0.18712 (7)
35	35	3.5	0.778 (16)	0.766 (16)	–
		4.5	0.642 (12)	0.6321 (85)	–
		5.5	0.5260 (94)	0.510 (12)	0.5051 (20)
		6.5	0.4038 (86)	0.4038 (86)	0.398 (13)
		7.5	0.3109 (45)	0.3109 (45)	0.3109 (45)
		8.5	0.2379 (25)	0.2379 (25)	0.2379 (25)
		9.0	0.2112 (37)	0.2112 (37)	0.2112 (37)

with our previous calculations at 7 TeV without introducing any other source of discrepancy related to the change of the PDF set.

All numerical calculations were implemented in FORTRAN. Numerical integrations and the computation of the polygamma functions were performed using specific CERN program libraries [61]. Furthermore, we used slightly modified versions of the **Chyp** [62] and **Psi** [63] routines in order to perform the calculation of the Gauss hypergeometric function $_2F_1$ and of the real part of the ψ function, respectively.

The most significant source of uncertainty is the numerical four-dimensional integration over the variables $|\vec{k}_{J_1}|$, $|\vec{k}_{J_2}|$, y_{J_1}, and ν, which was directly estimated by **Dadmul** integration routine [61]. In a recent paper [31], we have shown that the other two sources, which are, respectively, the one-dimensional integration over the longitudinal momentum fraction ζ in the NLO impact factors $c_{1,2}^{(1)}(n, \nu, |\vec{k}_{J_{1,2}}|, x_{J_{1,2}})$

Table 5 Values of C_3/C_0 from the "exact" BLM method, for all choices of the cuts on jet transverse momenta and of the central rapidity region (see Fig. 6)

$k_{J_1,\min}$ (GeV)	$k_{J_2,\min}$ (GeV)	Y	$y_{\max}^C = 0$	$y_{\max}^C = 1.5$	$y_{\max}^C = 2.5$
20	20	3.5	0.593 (22)	0.577 (19)	–
		4.5	0.432 (13)	0.425 (14)	–
		5.5	0.308 (12)	0.305 (15)	0.3019 (68)
		6.5	0.2139 (67)	0.2139 (67)	0.210 (18)
		7.5	0.1439 (29)	0.1439 (29)	0.1439 (29)
		8.5	0.0954 (17)	0.0954 (17)	0.0954 (17)
		9.0	0.0775 (13)	0.0775 (13)	0.0775 (13)
20	30	3.5	0.551 (26)	0.544 (14)	–
		4.5	0.3950 (88)	0.3896 (97)	–
		5.5	0.281 (13)	0.278 (12)	0.276 (3)
		6.5	0.1973 (48)	0.1973 (48)	0.194 (14)
		7.5	0.1389 (49)	0.1389 (49)	0.1389 (49)
		8.5	0.0944 (13)	0.0944 (13)	0.0944 (13)
		9.0	0.0795 (25)	0.0795 (25)	0.0795 (25)
20	35	3.5	0.555 (19)	0.528 (15)	–
		4.5	0.377 (11)	0.3724 (94)	–
		5.5	0.2652 (90)	0.263 (10)	0.2599 (30)
		6.5	0.1842 (48)	0.1842 (48)	0.184 (11)
		7.5	0.1272 (24)	0.1272 (24)	0.1272 (24)
		8.5	0.0888 (11)	0.0888 (11)	0.0888 (11)
		9.0	0.0756 (12)	0.0756 (12)	0.0756 (12)
20	40	3.5	0.529 (18)	0.520 (21)	–
		4.5	0.364 (10)	0.3585 (79)	–
		5.5	0.2496 (80)	0.249 (11)	0.2400 (40)
		6.5	0.1717 (41)	0.1717 (41)	0.171 (13)
		7.5	0.1188 (18)	0.1188 (18)	0.1188 (18)
		8.5	0.0836 (66)	0.0836 (66)	0.0836 (66)
		9.0	0.0720 (52)	0.0720 (52)	0.0720 (52)
35	35	3.5	0.6478 (76)	0.6360 (95)	–
		4.5	0.4983 (75)	0.4887 (40)	–
		5.5	0.3690 (55)	0.3652 (69)	0.3613 (84)
		6.5	0.2648 (47)	0.2648 (47)	0.2596 (93)
		7.5	0.1838 (17)	0.1838 (17)	0.1838 (17)
		8.5	0.1257 (16)	0.1257 (16)	0.1257 (16)
		9.0	0.1043 (12)	0.1043 (12)	0.1043 (12)

Table 6 Values of C_2/C_1 from the "exact" BLM method, for all choices of the cuts on jet transverse momenta and of the central rapidity region (see Fig. 7)

$k_{J_1,\min}$ (GeV)	$k_{J_2,\min}$ (GeV)	Y	$y_{\max}^C = 0$	$y_{\max}^C = 1.5$	$y_{\max}^C = 2.5$
20	20	3.5	0.759 (21)	0.749 (28)	–
		4.5	0.671 (26)	0.665 (28)	–
		5.5	0.583 (17)	0.583 (37)	0.580 (24)
		6.5	0.506 (21)	0.506 (21)	0.484 (27)
		7.5	0.4278 (55)	0.4278 (55)	0.4278 (55)
		8.5	0.3576 (91)	0.3576 (91)	0.3576 (91)
		9.0	0.3236 (27)	0.3236 (27)	0.3236 (27)
20	30	3.5	0.724 (23)	0.727 (25)	–
		4.5	0.642 (15)	0.638 (18)	–
		5.5	0.563 (23)	0.559 (27)	0.561 (11)
		6.5	0.491 (13)	0.491 (13)	0.489 (34)
		7.5	0.4245 (83)	0.4245 (83)	0.4245 (83)
		8.5	0.3644 (54)	0.3644 (54)	0.3644 (54)
		9.0	0.3377 (67)	0.3377 (67)	0.3377 (67)
20	35	3.5	0.713 (19)	0.710 (24)	–
		4.5	0.622 (21)	0.623 (22)	–
		5.5	0.542 (14)	0.542 (22)	0.5414 (50)
		6.5	0.473 (17)	0.473 (17)	0.470 (29)
		7.5	0.4095 (50)	0.4095 (50)	0.4095 (50)
		8.5	0.3548 (63)	0.3548 (63)	0.3548 (63)
		9.0	0.3299 (31)	0.3299 (31)	0.3299 (31)
20	40	3.5	0.697 (18)	0.695 (16)	–
		4.5	0.612 (17)	0.607 (17)	–
		5.5	0.523 (10)	0.526 (24)	0.5256 (96)
		6.5	0.459 (12)	0.459 (12)	0.455 (33)
		7.5	0.3960 (33)	0.3960 (33)	0.3960 (33)
		8.5	0.3441 (45)	0.3441 (45)	0.3441 (45)
		9.0	0.3224 (12)	0.3224 (12)	0.3224 (12)
35	35	3.5	0.809 (16)	0.805 (14)	–
		4.5	0.728 (14)	0.7247 (98)	–
		5.5	0.659 (13)	0.644 (14)	0.6421 (27)
		6.5	0.562 (12)	0.563 (12)	0.561 (19)
		7.5	0.4799 (67)	0.4799 (67)	0.4799 (67)
		8.5	0.3984 (40)	0.3984 (40)	0.3984 (40)
		9.0	0.3588 (61)	0.3588 (61)	0.3588 (61)

(see Eqs. (36) and (37) of Ref. [25]) and the upper cutoff in the numerical integrations over $|\vec{k}_{J_1}|$, $|\vec{k}_{J_2}|$, and ν, are negligible with respect to the first one. For this reason the error bars of all predictions presented in this work are just those given by the `Dadmul` routine.

We summarize our results in Tables 1, 2, 3, 4, 5, 6, 7 and in Figs. 2, 3, 4, 5, 6, 7, 8. From Table 1 (and Fig. 2) we can see that the different variants of implementation of the BLM method give predictions which deviate at the

level of $\sim$10 % for C_0 and at the level of $\sim$5 % for C_1/C_0, while they basically agree within errors for all other ratios R_{nm}. For this reason, all remaining tables (and figures) refer to the "exact" BLM case only. Table 2 (and Fig. 3) show, quite reasonably, that for all choices of the cuts on jet transverse momenta, the larger is $y_{\max}^C$, the lower is the total cross section C_0, up the value of Y is reached where the presence of cut of the central rapidity region becomes ineffective. All remaining tables (and figures) unan-

Table 7 Values of C_3/C_2 from the "exact" BLM method, for all choices of the cuts on jet transverse momenta and of the central rapidity region (see Fig. 8)

$k_{J_1,\min}$ (GeV)	$k_{J_2,\min}$ (GeV)	Y	$y^{\mathrm{C}}_{\max} = 0$	$y^{\mathrm{C}}_{\max} = 1.5$	$y^{\mathrm{C}}_{\max} = 2.5$
20	20	3.5	0.792 (22)	0.790 (26)	–
		4.5	0.727 (30)	0.731 (32)	–
		5.5	0.673 (24)	0.672 (49)	0.671 (26)
		6.5	0.611 (28)	0.611 (28)	0.634 (55)
		7.5	0.5509 (92)	0.5509 (92)	0.5509 (92)
		8.5	0.492 (16)	0.492 (16)	0.492 (16)
		9.0	0.4627 (59)	0.4627 (59)	0.4627 (59)
20	30	3.5	0.758 (37)	0.756 (23)	–
		4.5	0.687 (18)	0.689 (22)	–
		5.5	0.625 (32)	0.629 (36)	0.628 (11)
		6.5	0.566 (18)	0.567 (18)	0.566 (54)
		7.5	0.518 (22)	0.518 (22)	0.518 (22)
		8.5	0.4530 (93)	0.4530 (93)	0.4530 (93)
		9.0	0.424 (17)	0.424 (17)	0.424 (17)
20	35	3.5	0.741 (19)	0.740 (23)	–
		4.5	0.670 (24)	0.671 (23)	–
		5.5	0.609 (15)	0.610 (32)	0.6090 (25)
		6.5	0.547 (21)	0.547 (21)	0.555 (43)
		7.5	0.4887 (75)	0.4887 (75)	0.4887 (75)
		8.5	0.4312 (86)	0.4312 (86)	0.4312 (86)
		9.0	0.4033 (50)	0.4033 (50)	0.4033 (50)
20	40	3.5	0.728 (19)	0.732 (32)	–
		4.5	0.650 (18)	0.657 (18)	–
		5.5	0.591 (15)	0.592 (34)	0.578 (13)
		6.5	0.524 (17)	0.524 (17)	0.532 (56)
		7.5	0.4700 (63)	0.4700 (63)	0.4700 (63)
		8.5	0.4134 (62)	0.4134 (62)	0.4134 (62)
		9.0	0.3850 (25)	0.3850 (25)	0.3850 (25)
35	35	3.5	0.832 (13)	0.830 (11)	–
		4.5	0.776 (14)	0.7731 (94)	–
		5.5	0.701 (13)	0.716 (18)	0.7152 (27)
		6.5	0.656 (16)	0.656 (16)	0.652 (31)
		7.5	0.5912 (88)	0.5912 (88)	0.5912 (88)
		8.5	0.5284 (96)	0.5284 (96)	0.5284 (96)
		9.0	0.4939 (11)	0.4939 (11)	0.4939 (11)

imously show that all ratios R_{nm} remain unaffected by the cut on the central rapidity region, over the entire region of values of Y. This is obvious for the values of Y large enough to be insensitive to the very presence of a non-zero $y^{\mathrm{C}}_{\max}$, but it is unexpectedly true also for the lower values of Y.

The latter point means that in our approach, i.e. NLA BFKL with BLM optimization, the cut on jet central rapidities leads to a proportional reduction of both the total cross section, C_0, and the other coefficients C_1, C_2, C_3, which parametrize the azimuthal angle distribution. In other words in our approach, the central cut only reduces the value of the total cross section, but does not affect the azimuthal angle distribution of dijets. It would be very interesting to study whether such feature remains true also in other approaches, both within the BFKL approach, but using different ideas about the inclusion of the physics beyond NLA, and also in other, non-BFKL schemes, like fixed-order DGLAP or approaches using k_T-factorization for the central jet production.
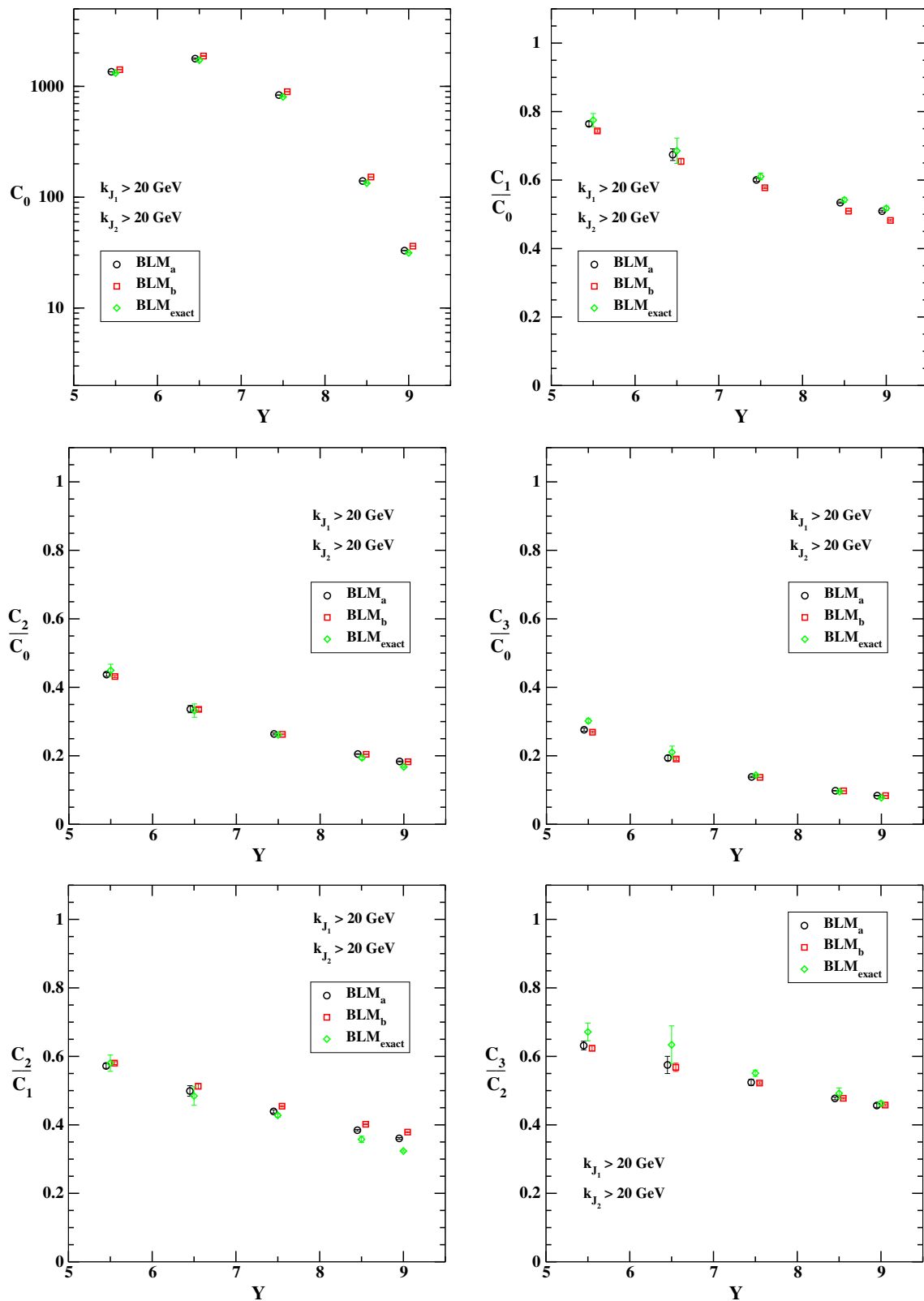
Fig. 2 Y-dependence of C_0 and of several ratios C_m/C_n for $k_{J_1,\min} = k_{J_2,\min} = 20\,\text{GeV}$ and for $y_{\max}^{\text{C}} = 2.5$, from the three variants of the BLM method (data points have been slightly shifted along the *horizontal axis* for the sake of readability; see Table 1)
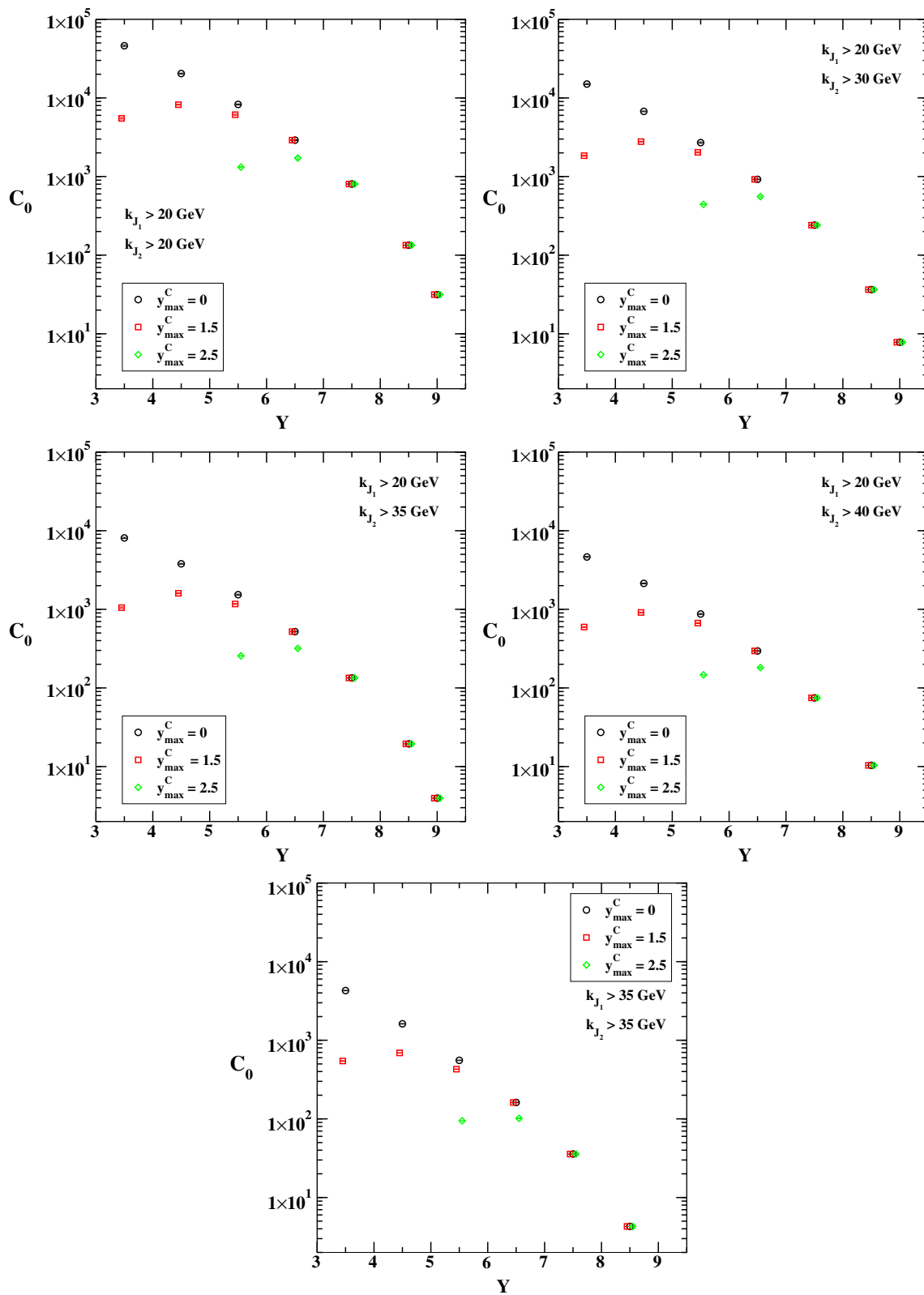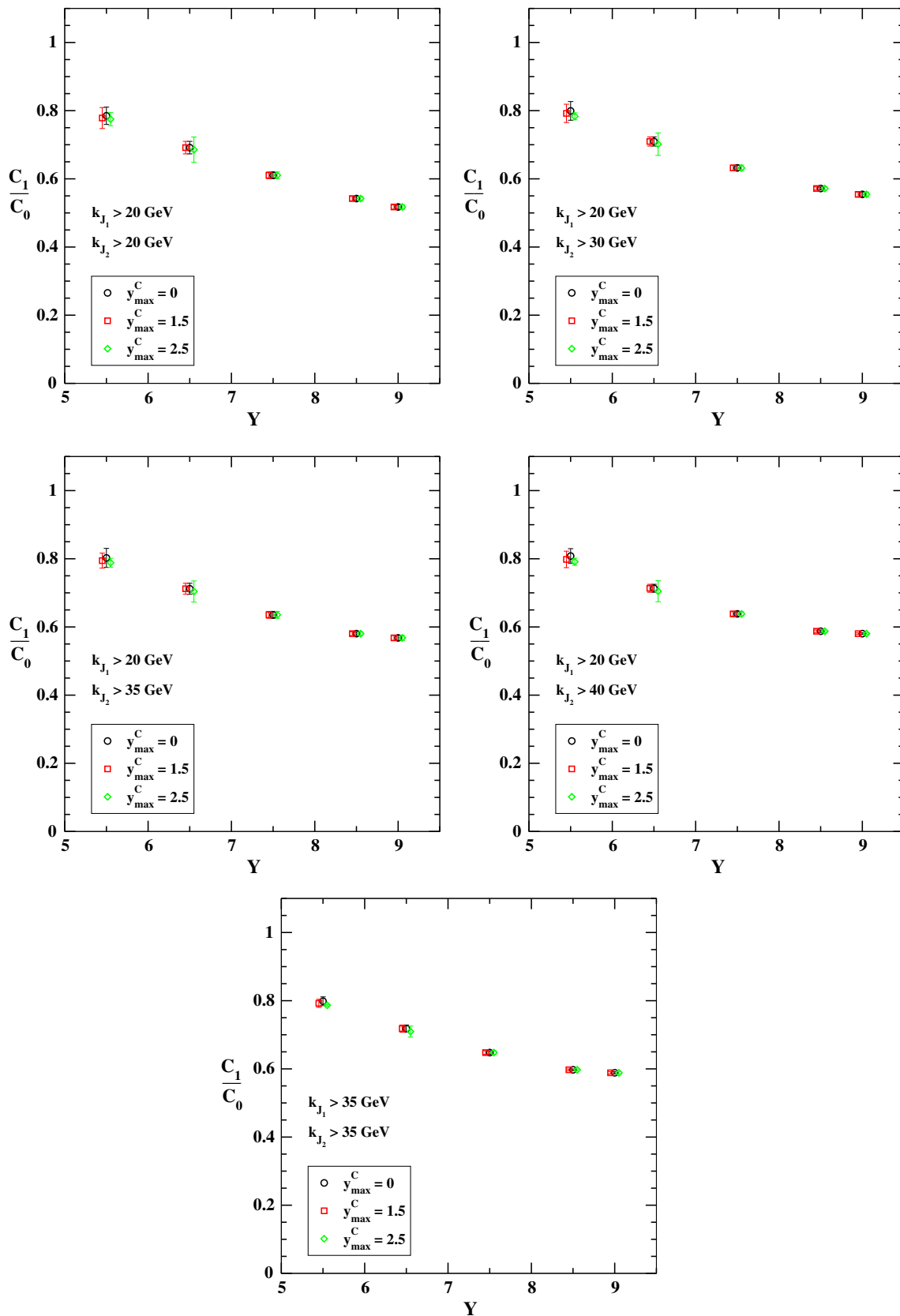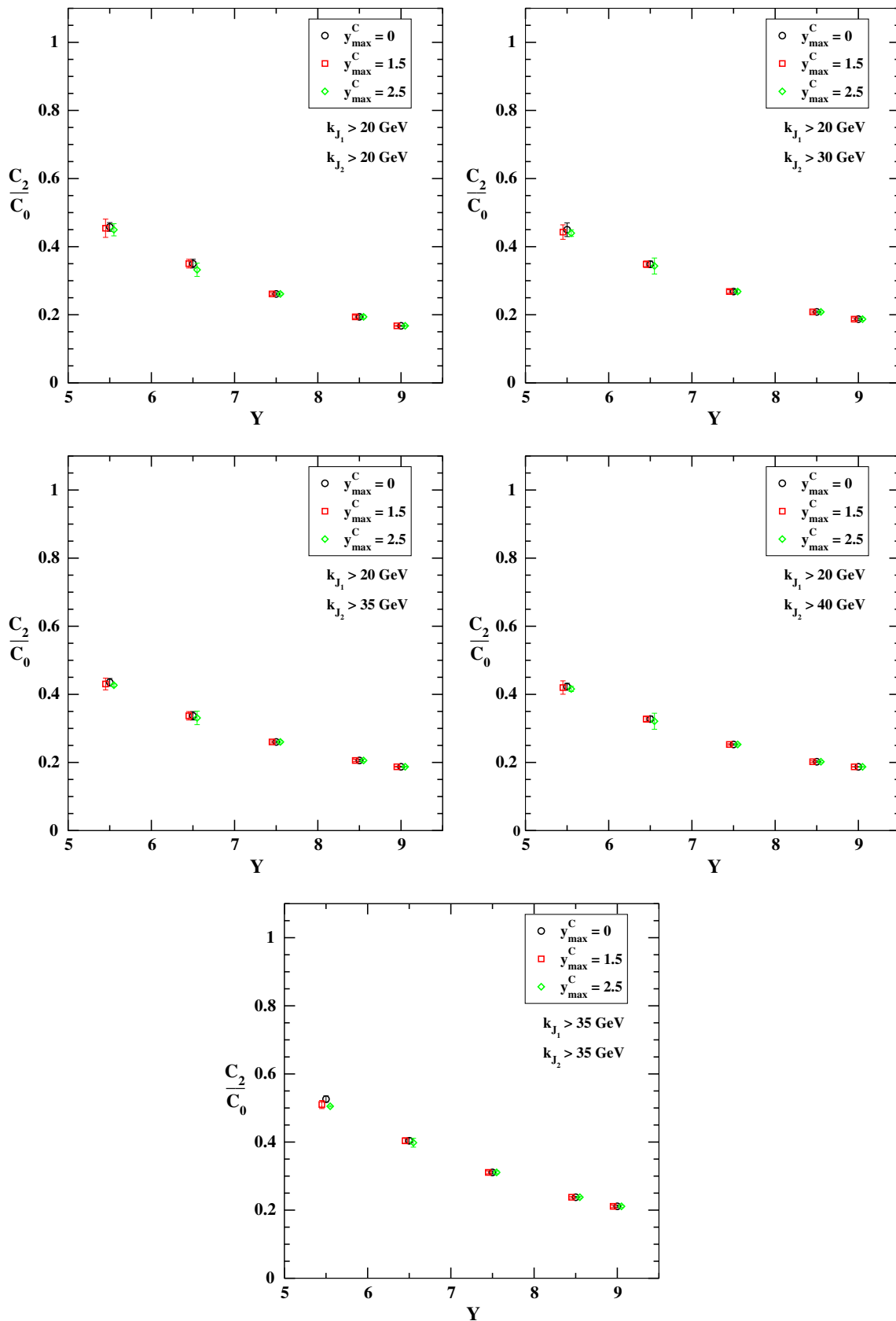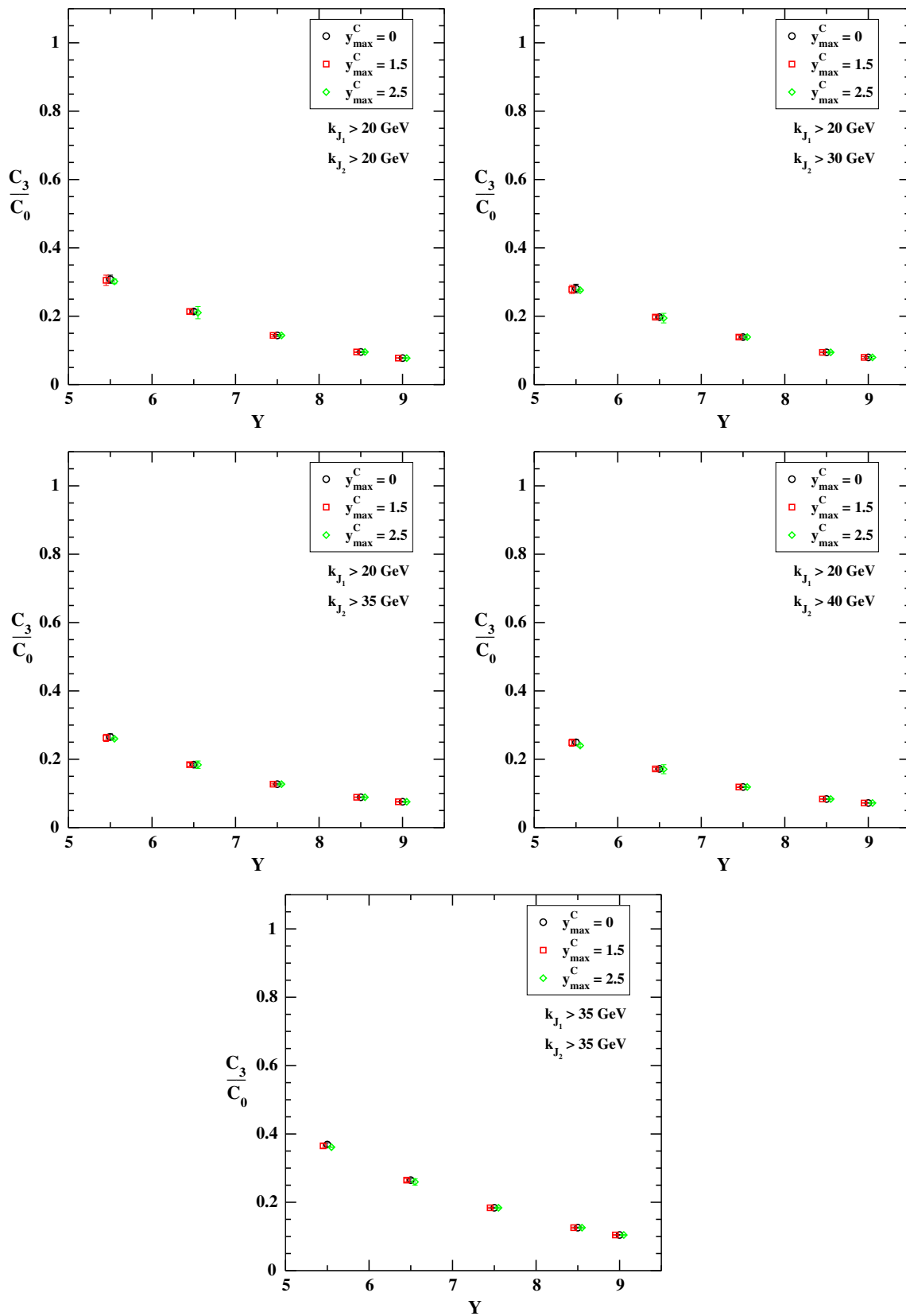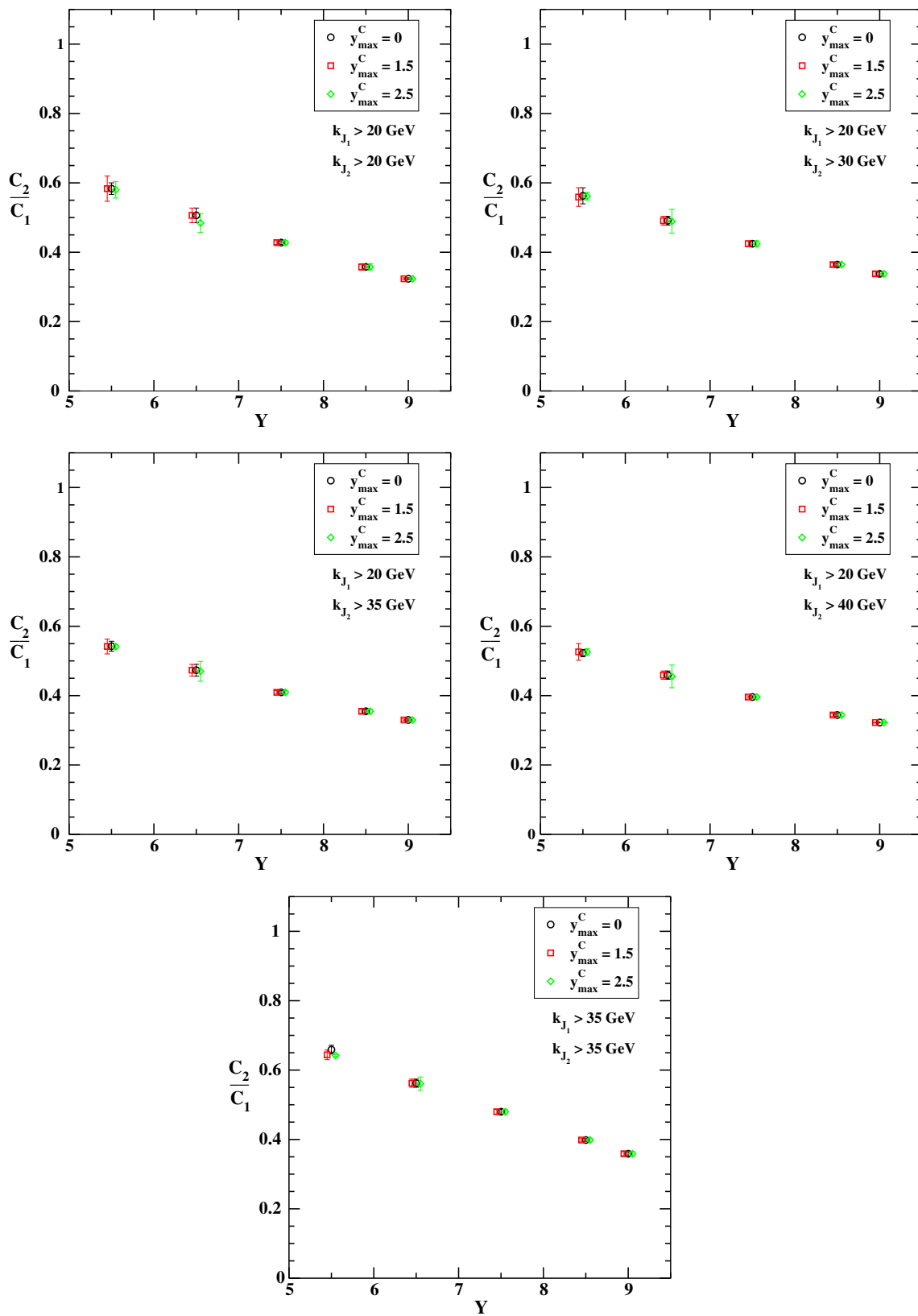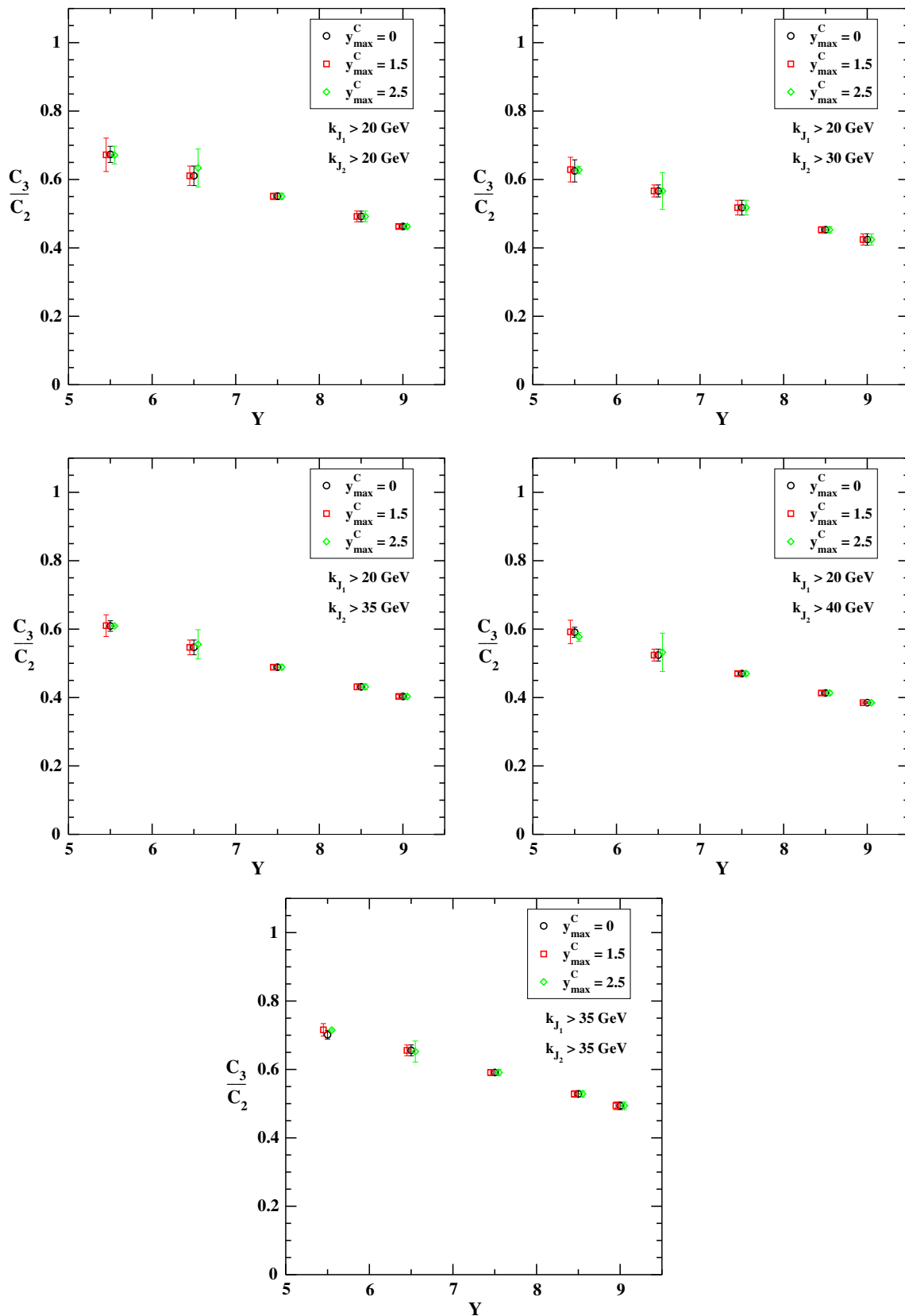
Fig. 3 Y-dependence of C_0 from the "exact" BLM method, for all choices of the cuts on jet transverse momenta and of the central rapidity region (data points have been slightly shifted along the *horizontal axis* for the sake of readability; see Table 2)

Fig. 4 Y-dependence of C_1/C_0 from the "exact" BLM method, for all choices of the cuts on jet transverse momenta and of the central rapidity region (data points have been slightly shifted along the *horizontal axis* for the sake of readability; see Table 3)

Fig. 5 Y-dependence of C_2/C_0 from the "exact" BLM method, for all choices of the cuts on jet transverse momenta and of the central rapidity region (data points have been slightly shifted along the *horizontal axis* for the sake of readability; see Table 4)

Fig. 6 Y-dependence of C_3/C_0 from the "exact" BLM method, for all choices of the cuts on jet transverse momenta and of the central rapidity region (data points have been slightly shifted along the *horizontal axis* for the sake of readability; see Table 5)

Fig. 7 Y-dependence of C_2/C_1 from the "exact" BLM method, for all choices of the cuts on jet transverse momenta and of the central rapidity region (data points have been slightly shifted along the *horizontal axis* for the sake of readability; see Table 6)

Fig. 8 Y-dependence of C_3/C_2 from the "exact" BLM method, for all choices of the cuts on jet transverse momenta and of the central rapidity region (data points have been slightly shifted along the *horizontal axis* for the sake of readability; see Table 7)

4 Conclusions

In this paper we have considered the Mueller–Navelet jet production process at LHC at the center-of-mass energy of 13 TeV and have produced predictions for total cross sections and several azimuthal correlations and ratios between them in full NLA BFKL approach, in a theoretical setup in which jet vertices where taken in the so-called "small-cone approximation" and the BFKL series was optimized adopting the BLM method to fix, at a common value, the renormalization and the factorization scales.

It is well known that BFKL predictions for the Mueller–Navelet process suffer from large uncertainties due to basically our disability to resum BFKL energy logarithms beyond NLA in a model-independent way. In this situation one needs to rely on some approaches to optimization of perturbative series. Here we have used the BLM method which was previously quite successful in describing the LHC 7 TeV data on jet angular correlations. We hope that the forthcoming LHC analysis at 13 TeV will shed a new light on the issue and will allow one to better discriminate among theoretical ideas about the BFKL physics beyond the NLA approximation. In this respect we believe that it could be advantageous if the comparison of theory predictions with the data would be done in a kinematic range where theoretical calculations do not have other uncertainties except the ones mentioned above.

Therefore here, differently from all previous studies of the same kind, we considered in our analysis the effect of excluding the possibility that one of the two detected jets be produced in the central rapidity region. Central jets originate from small-x partons, and the collinear approach for the description of the Mueller–Navelet jet vertices may be not good at small x. The outcome of our analysis is that for two reasonable ways to define the extension of the central region: a) the total cross section, C_0, is strongly reduced by the "exclusion cuts" in the range ($Y < 5.5$) where they are effective; b) on the other hand, in the same kinematics, the difference with respect to the case of no central rapidity exclusion is invisible in azimuthal correlations and in ratios between them.

We believe that it would be very interesting to confront these conclusions with LHC data.

References

1. A.H. Mueller, H. Navelet, Nucl. Phys. B **282**, 727 (1987)
2. V.S. Fadin, E.A. Kuraev, L.N. Lipatov, Phys. Lett. B **60**, 50 (1975)
3. E.A. Kuraev, L.N. Lipatov, V.S. Fadin, Zh. Eksp. Teor. Fiz. **71**, 840 (1976) [Sov. Phys. JETP **44** (1976) 443]
4. E.A. Kuraev, L.N. Lipatov, V.S. Fadin, **72**, 377 (1977) [45 (1977) 199]
5. Ya.Ya. Balitskii, L.N. Lipatov, Sov. J. Nucl. Phys. **28**, 822 (1978)
6. V.S. Fadin, L.N. Lipatov, Phys. Lett. B **429**, 127 (1998). arXiv:hep-ph/9802290
7. M. Ciafaloni, G. Camici, Phys. Lett. B **430**, 349 (1998). arXiv:hep-ph/9803389
8. V.S. Fadin, R. Fiore, A. Papa, Phys. Rev. D **60**, 074025 (1999). arXiv:hep-ph/9812456
9. V.S. Fadin, D.A. Gorbachev, Pisma v Zh. Eksp. Teor. Fiz. **71**, 322 (2000) [JETP Letters **71** (2000) 222]
10. V.S. Fadin, D.A. Gorbachev, Phys. Atom. Nucl. **63**, 2157 (2000) [Yad. Fiz. **63** (2000) 2253]
11. V.S. Fadin, R. Fiore, Phys. Lett. B **610**, 61 (2005) [Erratum-ibid. **621** (2005) 61] arXiv:hep-ph/0412386
12. V.S. Fadin, R. Fiore, Phys. Rev. D **72**, 014018 (2005). arXiv:hep-ph/0502045
13. V.N. Gribov, L.N. Lipatov, Sov. J. Nucl. Phys. **15**, 438 (1972)
14. G. Altarelli, G. Parisi, Nucl. Phys. B **126**, 298 (1977)
15. Y.L. Dokshitzer, Sov. Phys. JETP **46**, 641 (1977)
16. J. Bartels, D. Colferai, G.P. Vacca, Eur. Phys. J. C **24**, 83 (2002). arXiv:hep-ph/0112283
17. J. Bartels, D. Colferai, G.P. Vacca, Eur. Phys. J. C **29**, 235 (2003). arXiv:hep-ph/0206290
18. F. Caporale, D.Yu. Ivanov, B. Murdaca, A. Papa, A. Perri, JHEP **1202**, 101 (2012). arXiv:1112.3752 [hep-ph]
19. D.Yu. Ivanov, A. Papa, JHEP **1205**, 086 (2012). arXiv:1202.1082 [hep-ph]
20. M. Furman, Nucl. Phys. B **197**, 413 (1982)
21. F. Aversa, P. Chiappetta, M. Greco, J.P. Guillet, Nucl. Phys. B **327**, 105 (1989)
22. F. Aversa, P. Chiappetta, M. Greco, J.P. Guillet, Z. Phys. C **46**, 253 (1990)
23. D. Colferai, A. Niccoli, JHEP **1504**, 071 (2015). arXiv:1501.07442 [hep-ph]
24. D. Colferai, F. Schwennsen, L. Szymanowski, S. Wallon, JHEP **1012**, 026 (2010). arXiv:1002.1365 [hep-ph]
25. F. Caporale, D.Yu. Ivanov, B. Murdaca, A. Papa, Nucl. Phys. B **877**, 73 (2013). arXiv:1211.7225 [hep-ph]
26. F. Caporale, B. Murdaca, A. Sabio Vera, C. Salas. Nucl. Phys. B **875**, 134 (2013). arXiv:1305.4620 [hep-ph]
27. B. Ducloué, L. Szymanowski, S. Wallon, JHEP **1305**, 096 (2013). arXiv:1302.7012 [hep-ph]
28. B. Ducloué, L. Szymanowski, S. Wallon, Phys. Rev. Lett. **112**, 082003 (2014). arXiv:1309.3229 [hep-ph]
29. B. Ducloué, L. Szymanowski, S. Wallon, Phys. Lett. B **738**, 311 (2014). arXiv:1407.6593 [hep-ph]
30. F. Caporale, D.Yu. Ivanov, B. Murdaca, A. Papa, Eur. Phys. J. C **74**, 10, 3084 (2014) [Eur. Phys. J. C **75** (2015) 11, 535] arXiv:1407.8431 [hep-ph]
31. F.G. Celiberto, D.Yu. Ivanov, B. Murdaca, A. Papa, Eur. Phys. J. C **75**, 6, 292 (2015). arXiv:1504.08233 [hep-ph]
32. A. Sabio Vera, F. Schwennsen, Nucl. Phys. B **776**, 170 (2007). arXiv:hep-ph/0702158
33. A. Sabio Vera, Nucl. Phys. B **746**, 1 (2006). arXiv:hep-ph/0602250
34. B. Ducloue, L. Szymanowski, S. Wallon, Phys. Rev. D **92**, 7, 076002 (2015). arXiv:1507.04735 [hep-ph]

35. A.H. Mueller, L. Szymanowski, S. Wallon, B.W. Xiao, F. Yuan, arXiv:1512.07127 [hep-ph]
36. G.P. Salam, JHEP **9807**, 019 (1998). arXiv:hep-ph/9806482
37. M. Ciafaloni, D. Colferai, G.P. Salam, A.M. Stasto, Phys. Lett. B **587**, 87 (2004). arXiv:hep-ph/0311325
38. M. Ciafaloni, D. Colferai, G.P. Salam, A.M. Stasto, Phys. Rev. D **68**, 114003 (2003). arXiv:hep-ph/0307188
39. M. Ciafaloni, D. Colferai, G.P. Salam, A.M. Stasto, Phys. Lett. B **576**, 143 (2003). arXiv:hep-ph/0305254
40. M. Ciafaloni, D. Colferai, G.P. Salam, A.M. Stasto, Phys. Lett. B **541**, 314 (2002). arXiv:hep-ph/0204287
41. M. Ciafaloni, D. Colferai, G.P. Salam, A.M. Stasto, Phys. Rev. D **66**, 054014 (2002). arXiv:hep-ph/0204282
42. M. Ciafaloni, D. Colferai, G.P. Salam, JHEP **0007**, 054 (2000). arXiv:hep-ph/0007240
43. M. Ciafaloni, D. Colferai, G.P. Salam, JHEP **9910**, 017 (1999). arXiv:hep-ph/9907409
44. M. Ciafaloni, D. Colferai, G.P. Salam, Phys. Rev. D **60**, 114036 (1999). arXiv:hep-ph/9905566
45. M. Ciafaloni, D. Colferai, Phys. Lett. B **452**, 372 (1999). arXiv:hep-ph/9812366
46. A. Sabio Vera, Nucl. Phys. B **722**, 65 (2005). arXiv:hep-ph/0505128
47. J. Kwiecinski, L. Motyka, Phys. Lett. B **462**, 203 (1999). arXiv:hep-ph/9905567
48. P.M. Stevenson, Phys. Lett. B **100**, 61 (1981)
49. P.M. Stevenson, Phys. Rev. D **23**, 2916 (1981)
50. G. Grunberg, Phys. Lett. B **95**, 70 (1980) [Erratum-ibid. B **110** (1982) 501]
51. G. Grunberg, Phys. Lett. B **114**, 271 (1982)
52. G. Grunberg, Phys. Rev. D **29**, 2315 (1984)
53. S.J. Brodsky, G.P. Lepage, P.B. Mackenzie, Phys. Rev. D **28**, 228 (1983)
54. F. Caporale, D.Yu. Ivanov, B. Murdaca, A. Papa, Phys. Rev. D **91**, 11, 114009 (2015). arXiv:1504.06471 [hep-ph]
55. J. Currie, A. Gehrmann-De Ridder, E.W.N. Glover, J. Pires, JHEP **1401**, 110 (2014). arXiv:1310.3993 [hep-ph]
56. J. Bartels, A. Sabio Vera, F. Schwennsen, JHEP **0611**, 051 (2006). arXiv:hep-ph/0608154
57. S. Sapeta, arXiv:1511.09336 [hep-ph]
58. CMS Collaboration, S. Chatrchyan et al., CMS PAS FSQ-12-002 (2013)
59. A.D. Martin, W.J. Stirling, R.S. Thorne, G. Watt, Eur. Phys. J. C **63**, 189 (2009). arXiv:0901.0002 [hep-ph]
60. L.A. Harland-Lang, A.D. Martin, P. Motylinski, R.S. Thorne, Eur. Phys. J. C **75**, 5, 204 (2015). arXiv:1412.3989 [hep-ph]
61. CERNLIB Homepage: http://cernlib.web.cern.ch/cernlib
62. R. Forrey, J. Comput. Phys. **137**, 79 (1997)
63. W.J. Cody, A.J. Strecok, H.C. Thacher, Math. Comput. **27**, 121 (1973)